Inhibiting IRE-1 RNase signaling decreases HIV-1 Tat-induced inflammatory M1 state in microglial cells

Douglas Bardini Silveira (douglas.bardini@posgrad.ufsc.br)
Universidade Federal de Santa Catarina
Aguinaldo Roberto Pinto
Universidade Federal de Santa Catarina
Monique Ferrary
Universidade Federal de Santa Catarina
Hernán Terenzi
Universidade Federal de Santa Catarina

Short Report

Keywords: HIV-1 Tat, ER stress, IRE1, XBP-1, HAND, Microglia

Posted Date: April 19th, 2022

DOI: https://doi.org/10.21203/rs.3.rs-1443224/v2

Abstract

HIV-1 transactivator (Tat) protein plays a critical role in neurological disorders resulting from viral infection, commonly known as HIV-1-associated neurocognitive disorders (HAND). Previous studies have shown tha circulant Tat induces M1 microglial activation, one of the hallmark features of HAND, and this is coupled with ER stress and subsequent Unfolded Protein Response (UPR) deflagration. Here, we demonstrate that bystander stimuli of Tat in microglial cells result in the simultaneous overexpression of IRE1-related markers and production of M1-typed pro-inflammatory mediators. We also show that blocking IRE1/XBP-1 signaling using 4μ8C diminishes such inflammatory response. These findings reinforce a role for the IRE1/XBP-1 pathway in HIV-1 neuropathology and suggest that targeting IRE1 RNase activity using 4μ8C or analogue compounds may provide a therapeutic intervention to mitigate against neuroinflammation in HAND.

1. Introduction

The human immunodeficiency virus type 1 (HIV-1) trans-activator (Tat) protein is a key mediator in the development of HIV-1-associated neurocognitive disorders (HAND). Extracellular Tat is biologically active and continually secreted from infected cells even under antiretroviral therapy [1–3]. Once circulating Tat is able to enter the central nervous system (CNS) and can interact with a broad range of cell types leading to dysregulated gene expression, chronic cell activation, inflammation, neurotoxicity, and structural brain damage [4–6]. In microglial cells, the immune ‘arm’ of the CNS Tat can drive their transition from a wound healing, neuroprotective M2 microglial phenotype to an inflammatory M1 state characterized by overexpression of neuroinflammation mediators and co-stimulatory surface proteins [8–9]. Increased M1-like microglia is consistent with high levels of neurodegeneration observed in peopl e living with HIV-1 and may potentially play a central role in the pathophysiology of HAND [9].

Most neurodegenerative disorders, regardless of what triggered them could conceivably be viewed as arising from defective protein folding and chronic impairment of endoplasmic reticulum (ER) homeostasis. Perturbations in the ER folding environment elicit a coordinated molecular response that involves several adaptive signaling pathways, commonly termed unfolded protein response (UPR) [10], which likely has a critical role in HIV-associated neurodegeneration [11–13]. The UPR is canonically mediated by ER-transmembrane proteins, among which the Inositol-Requiring Enzyme 1 (IRE1) is its most conserved branch. IRE1 senses disturbances in ER homeostasis via its luminal domain, resulting in a conformational change and activation of both its cytoplasmic protein kinase and its RNAse domain. In turn, IRE1 activation leads to cleavage and subsequent ligation of the mRNA encoding the X-box binding protein-1 (XBP1), triggering the synthesis of a truncated and transcriptionally active spliced form of XBP1 (XBP1s) [14]. In an attempt to relieve ER stress, XBP1s enhance the transcription of genes that facilitate protein folding. IRE1 RNase also can cleave ER-localized mRNAs at a consensus site that is similar to the one found in XBP-1 splicing which limits protein translation, in a adaptive mechanism termed “regulated IRE1-dependent decay” (RIDD) [15]. Nonetheless continuous IRE1 activation can lead to inflammatory states and/or programmed cell death by triggering multiple signaling pathways [14–16].

In this study, we hypothesize that HIV-1 Tat-induced microglial M1 state can be regulated by disrupting IRE1 signaling and the subsequent ER stress alleviation. To investigate this, we modulated UPR in a previously established Tat-activated microglial model by using 4μ8C (7-hydroxy-4-methyl-2-oxo-2H-chromene-8-carbaldehyde), an aromatic aldehyde that binds to IRE1's RNAse domain and inhibits its activity. Our findings demonstrate that inhibition of the IRE1-XBP-1 pathway significantly suppresses the M1 microglial profile evoked by Tat, shedding light on the possibility that IRE1 RNAse inhibitors might be a feasible strategy to attenuate neuroinflammation and neuronal injury in HIV-1-positive individuals.

2. Material And Methods

2.1 Cell culture and experimental agents:

Recombinant HIV-1 Tat protein (full-length HIV-1 Tat clade B sequence, isolate BH10, UniProtKB - P69697, TAT_HV1B1) was produced and purified as described in Silveira et al [7]. BV-2 microglial cells were purchase from Banco de Células do Rio de Janeiro (Brazil), and maintained in Dulbecco's Modified Eagle's Medium (Sigma-Aldrich, USA) supplemented with 10% of heat-inactivated fetal bovine serum (Cultilab, Brazil), 1mM sodium pyruvate, 2 mM L-glutamine, at 37°C in 5% CO2. Cells were seeded ($5x10^6$) in 12-well plates and cultured until they reached 80-100% of confluency for experiments, when media was replaced by serum-free medium. The IRE1 inhibitor 4μ8C was purchased from Tocris Bioscience (Minneapolis, USA, #4479/50). For experiments targeting IRE1 inhibition, the small-molecule 4μ8C was solubilized according to supplier's instructions and assayed using a range of different concentrations with or without recombinant Tat, at different time-points. Heat-inactivated recombinant Tat (boiled at 90° C for 1 h) was used as an experimental control of non-stimulation.

2.2 Cell viability and apoptosis assessment:

BV-2 cells were assayed as described above and 100 μL of MTT [3-(4,5-Dimethyl-2-thiazolyl)-2,5-diphenyl-2H-tetrazolium bromide, Merck KGaA, Germany] solution (5 mg/mL in DMEM without serum) was added to each well. After 4 h incubation, supernatants were removed and 1 mL of dimethyl sulphoxide (Sigma-Aldrich, USA) was added to each well. Levels of MTT reduction were spectrophotometrically measured at 540 nm (SpectraMax Paradigm Multi-mode Microplate Reader, Molecular Devices, LLC, USA). In addition, the apoptotic profile of BV-2 cells was assessed by FITC Annexin V Apoptosis Detection Kit with 7-AAD (Biolegend, USA). Apoptotic cells were analyzed in FACSCanto II flow cytometer (Becton & Dickinson, USA) and FlowJo-VX software. Double-stained cells (late apoptotic events) and Annexin V-stained cells (early apoptotic events) were considered.

2.3 Measurement of CD16/32 expression.

BV-2 cells were assayed as described, detached from plates after 48h and labelled with FITC anti-CD16/32 (Biolegend, USA, #101305, 1 μg/106 cells, 40 min at 4° C). Analyses were performed in BD

FACSCanto II flow cytometer (Becton & Dickinson, USA) and FlowJo-VX software.

2.4 Cytometric bead array and NO dosage.

BV-2 cells were assayed as described above and supernatants collected after 48 h to assess inflammatory-related molecules using the CBA Mouse Inflammation kit (BD Pharmingen, USA) according to the supplier´s protocol. For NO dosage, supernatants were processed as previously described [7]. In brief, supernatants were mixed (1:1) with 0.1% naphthyl ethylenediamine and 1% sulfanilamide in 5% phosphoric acid solution (Sigma-Aldrich, USA) for 5 min at room temperature in the dark. Absorbance was then measured at 540 nm using a spectrophotometer (SpectraMax Paradigm Multi-mode Microplate Reader, Molecular Devices, LLC, USA).

2.5 Western blotting analysis:

BV-2 cells were assayed as described above and lysed after 48 h for western blot. Total protein concentrations were quantified by Bradford assay (Bio-Rad, USA). Samples were loaded (50 µg) and separated in 15% SDS-PAGE gel, then transferred (3 h at 200 mA) onto a nitrocellulose filter membrane (Bio-Rad, USA). The membranes were incubated at room temperature with 5% nonfat milk for 1 h, followed by incubation with primary anti-XBP-1 (Abcam, USA, #ab37152, 1:500), anti-eIF2α (Santa Cruz Biotechnology, USA, #sc-133132, 1:500), anti-p-eIF2α (Thermo Fischer, USA, #44-728G, 1:1000) or anti-β-actin (Abcam, USA, #ab8227, 1:5000). Membranes were then incubated with goat anti-rabbit (Sigma-Aldrich, USA, #A0545, 1:5000) or goat anti-mouse (Sigma-Aldrich, USA, #A9309, 1:1000) secondary antibodies in skimmed milk for 1 h at room temperature. ECL Western blot substrates (Pierce, Thermo Fisher Scientific, USA) were used to identify immunoreactive bands and analyzed using ImageJ software (http://rsbweb.nih.gov/ij/).

2.6 Quantitative real-time PCR:

Total RNA was isolated from cells using a RNeasy Mini Kit (Qiagen, USA) and qRT-PCR was performed on a StepOne Real-Time PCR System (Applied Biosystems, Life Technologies, USA) using a FastSYBR® Green PCR Master Mix (Applied Biosystems, Life Technologies, USA). Reactions were performed in triplicate and the relative expression ratios calculated. Primer sequences were used as previously published [7].

2.7 Statistical analysis:

Statistical significance was evaluated using Student’s t test when considering differences between two experimental groups, or by one-way analysis of variance (ANOVA) followed by Tukey’s post hoc test in case of multiple groups. Statistical significance level was determined at $p < 0.05$.

3. Results

Given that higher concentrations of 4μ8C are suggested to affect cell proliferation, apoptosis and UPR-related signaling independently of its IRE1 RNase activity [16–17], we first sought to investigate whether 4μ8C impacts the kinetics of cell viability/apoptosis in microglia-like BV-2 cells under different concentrations. As shown in Fig. 1, incubation with 4μ8C substantially decreases MTT cleavage activity starting at 60 μM after 48 h, although lower concentrations did not induce changes over time (Fig. 1A). Also, the presence of IRE1 inhibitor at 10 μM did not affect MTT reduction and viability rates for BV-2 cells during ER stress evoked by recombinant Tat after 48 h (Fig. 1B and 1C), indicating absence of off-target effects on cellular survival. This intermediate time-point and 4μ8C dosing have been previously characterized as optimal assaying conditions for Tat-mediated ER stress assessments in BV-2 cell models [7] and 4μ8C inhibition of IRE1 RNase activity [16]. As such, these conditions were chosen for all subsequent experiments.

We next verified whether 4μ8C could modulate IRE1-mediated signaling and the expression of UPR in Tat-ER stressed BV-2 cells. The use of this inhibitor markedly downregulated IRE1 gene expression, both transcriptional forms of XBP-1, and the UPR-related early effector BIP (Binding Immunoglobulin Protein) in Tat-treated cell groups (Fig. 2A). At 10μM, 4μ8C was able to decrease Tat-induced XBP-1u (unspliced form) and XBP-1s (spliced form) protein levels (Fig. 2B), further confirming a blocking in IRE1 signaling driven by Tat. Importantly, there were no remarkable changes in gene expression for ATF4 (Activation Transcription Factor 4), CHOP (Homologous Protein C/EBP), and eIF2-α (Eukaryotic Translation Initiation Factor 2 Alpha) or in levels of eIF2-α phosphorylation – all such mediators are triggered downstream of both ER stress sensors PERK (Protein kinase R-like ER kinase) and ATF6 (Activating transcription factor 6), thus supporting a selective disruption of IRE1 RNase.

Finally, we sought to explore whether IRE1 RNase activity is involved in Tat-induced microglial inflammatory states by using 4μ8C IRE1 inhibitor. BV-2 cells were exposed to recombinant Tat in presence or absence of 10μM 4μ8C, and M1 phenotype markers were assessed. Levels of secreted NO, TNF-α and IL-6 (Fig. 3A) were significantly decreased by 4μ8C, hindering IRE1-dependent pathways. Such pharmacological inhibition of IRE1 RNase was also able to reduce the expression of surface CD16/32 triggered by recombinant Tat (Fig. 3B). We also analyzed gene expression of inducible NO synthase (iNOs) and compared it with expression levels for Arginase 1 (Arg-1), against which iNOs competes – these are common markers for M1 and non-inflammatory M2 phenotypes. Figure 3C shows, as expected, a significant decrease of iNOs levels concurrently with the lowering of Arg-1 gene expression elicited by recombinant Tat, reinforcing the role of IRE1 RNase in Tat-driven M1 microglial NO synthesis. Taken together, these results indicate a potential cross-talk between ER stress-related IRE1-XBP-1 signaling and M1 activation evoked by Tat in microglial cells.

4. Discussion

HAND refers to a spectrum of neurologic impairments which may emerge despite the currently available combined antiretroviral therapy [18]. Several reports have implied the progressive accumulation of misfolded proteins and their insufficient clearance rate in HIV-infected brains as a component of HAND pathogenesis [1–4]. Previous work has described there is an interplay between ER burden/UPR pathways and inflammogenic signaling, and this may be a central mechanism of M1-like activation of microglia and the infiltration of macrophages into CNS which is enabled by HIV or its soluble factors [19–20]. Moreover, we recently highlighted that circulant Tat stimuli leads to a coupled phenotype in microglial cells; PERK-dependent ER stress and inflammation responses [7]. In the present study, we interrogated the role of IRE1 RNase activity in mediating Tat-driven M1 microglial state by using a small-molecule inhibitor, 4μ8C.

IRE1 signaling has been extensively associated with cell death and inflammation in CNS. Compelling evidence of IRE1-triggered cascades in CNS-resident immune cells has been described in post-mortem samples of clinically confirmed cases of Alzheimer's disease, Huntington's disease, and glioma, as well in several in vivo and in vitro neurodegenerative diseases models [21]. The IRE1-XBP1s pathway also promotes astrocyte-intrinsic pro-inflammatory responses during experimental autoimmune encephalomyelitis, which is coordinated by trans-membrane chaperones placed in ER [22]. In addition, IRE1 RNase appears to be pivotal in microglia-mediated neuroinflammation, licensing a sustained release of pro-inflammatory cytokines and iNOS, and enabling NLRP3 inflammasome assembly [23–24]. IRE1 RNase also regulates IFN-I response in microglia, whose overactivation could induce a state of chronic neuroinflammation [25]. In line with such reports, we observed in our study a consistent activation of IRE1 branch in Tat-activated M1-like BV-2 cells, marked by growing expression of IRE1-linked genes and XBP-1 splicing and providing a formal connection between IRE1 activation and the underlying inflammatory effects of Tat on microglia. This potential coupling was further explored by pharmacological hindering of IRE1 RNase as discussed below.

The 4μ8C compound has been well-characterized as a selective inhibitor of IRE1 endonuclease based on reduced downstream splicing of XBP-1 in embryonic fibroblast, hepatoma and human multiple myeloma cell lines [16, 17, 26]. Here, we extend these findings by demonstrating an impaired IRE1-dependent response in 4μ8C-treated BV-2 cells, in parallel with an attenuation of M1 state under Tat activation. Although the present study was not designed to examine the mechanism by which IRE1/XBP-1 inhibition directly relieves BV-2 cells M1 activity over Tat exposure, our findings add new evidence for the modulation of the inflammatory programme in microglia by blocking IRE1 RNase domain. This statement is still coherent with previous studies demonstrating that both XBP-1s production and RIDD are induced in macrophages after stimulation and might work in sync to prevent M2 toward M1 phenotype shaping [27, 28]. It is worth noting also that the 10 uM 4μ8C dosing to inhibit IRE1 RNase activity had no effect on non-IRE1-related UPR components or cell viability, ruling out the involvement of off-target effects or cytotoxicity. The role of IRE1 RNase activity on M1 microglial skewing by soluble HIV-1 proteins should be further investigated in the future and might afford new insights into viral neuropathogenesis and therapeutics for neurologically affected HIV-1 individuals.

In conclusion, our work highlights IRE1/XBP-1 signaling as a regulator of microglial M1 polarization during Tat uptake and provides an important proof of concept to suggest the use of IRE1 RNase inhibitors as a platform for development of novel strategies to mitigate lasting neuroinflammation in HIV-1 infection. As well as useful tools for modulating IRE1 *in vitro* and *in vivo*, compounds like 4μ8C, or more pharmacologically suitable analogues, might be feasible for clinical applications in treatment of HAND or other neurodegenerative conditions.

Declarations

Funding

This research did not receive any specific grant from funding agencies in the public, commercial, or not-for-profit sectors. A.R.P. is a CNPq (Conselho Nacional de Desenvolvimento Científico e Tecnológico) scholar.

Conflict of Interest

The authors declare no conflicts of interest.

Authors Contributions

D.B.S. designed the study, performed experiments analyzed the data, and wrote the manuscript. M.F.A. performed experiments. H.T assisted in experiments, protein data analysing and resources providing. A.R.P designed the study, supervised the work and revised the manuscript. All authors read and approved the final version of the manuscript.

Data Availability Statement

The original data shown in this short communication are available from the corresponding author upon reasonable request.

Acknowledgments

We would like to express our gratitude to Dr. Gislaine Fongaro, Dr. Maristela M. Camargo, Dr. Rafael D. da Rosa and Dr. Oscar B. Romero for providing reagents and equipments, Natália Porto Flores for technical support and LAMEB/UFSC (Laboratório Multiusuário de Estudos em Biologia/Universidade Federal de Santa Catarina) for cell cytometry analysis. A.R.P. is a CNPq (Conselho Nacional de Desenvolvimento Científico e Tecnológico) scholar.

References

1. Marino J, Maubert ME, Mele AR, Spector C, Wigdahl B, Nonnemacher MR (2020). Functional impact of HIV-1 Tat on cells of the CNS and its role in HAND. Cell Mol Life Sci, 77(24):5079-5099.

doi:10.1007/s00018-020-03561-4

2. Dong H, Ye X, Zhong L, et al (2019). Role of FOXO3 Activated by HIV-1 Tat in HIV-Associated Neurocognitive Disorder Neuronal Apoptosis. Front Neurosci, 13. doi:10.3389/fnins.2019.00044
3. Saiyed ZM, Gandhi N, Agudelo M, et al (2011). HIV-1 Tat upregulates expression of histone deacetylase-2 (HDAC2) in human neurons: Implication for HIV-associated neurocognitive disorder (HAND). Neurochem Int, 58(6):656-664. doi:10.1016/j.neuint.2011.02.004
4. Wu X, Dong H, Ye X, et al (2018). HIV-1 Tat increases BAG3 via NF-κB signaling to induce autophagy during HIV-associated neurocognitive disorder. Cell Cycle, 17(13):1614-1623. doi:10.1080/15384101.2018.1480219
5. Campestrini J, Silveira DB, Pinto AR (2018). HIV-1 Tat-induced bystander apoptosis in Jurkat cells involves unfolded protein responses: Apoptosis in Jurkat cells mediated by Unfolded Protein Responses. Cell Biochem Funct, 36(7):377-386. doi:10.1002/cbf.3357
6. Marino J, Wigdahl B, Nonnemacher MR (2020). Extracellular HIV-1 Tat Mediates Increased Glutamate in the CNS Leading to Onset of Senescence and Progression of HAND. Front Aging Neurosci, 12. doi:10.3389/fnagi.2020.00168.
7. Silveira DB, Américo MF, Flores NP, Terenzi H, Pinto AR (2022). Pharmacological inhibition of UPR sensor PERK attenuates HIV Tat-induced inflammatory M1 phenotype in microglial cells. Cell Biochem Funct, 1-12. doi:10.1002/cbf.3685
8. Borrajo A, Spuch C, Penedo MA, Olivares JM, Agís-Balboa RC (2021). Important role of microglia in HIV-1 associated neurocognitive disorders and the molecular pathways implicated in its pathogenesis. Ann Med, 53(1):43-69. doi:10.1080/07853890.2020.1814962
9. Tang Y, Le W (2016). Differential roles of M1 and M2 microglia in neurodegenerative diseases. Mol Neurobiol, 53(2):1181-1194. doi:10.1007/s12035-014-9070-5
10. Hetz C, Zhang K, Kaufman RJ (2020). Mechanisms, regulation and functions of the unfolded protein response. Nat Rev Mol Cell Biol, 21(8):421-438. doi:10.1038/s41580-020-0250-z
11. Sprenkle NT, Sims SG, Sánchez CL, Meares GP (2017). Endoplasmic reticulum stress and inflammation in the central nervous system. Mol Neurodegener, 12(1). doi:10.1186/s13024-017-0183-y
12. Torkzaban B, Mohseni Ahooyi T, Duggan M, Amini S, Khalili K (2020). Cross-talk between lipid homeostasis and endoplasmic reticulum stress in neurodegeneration: Insights for HIV-1 associated neurocognitive disorders (HAND). Neurochem Int, 141(104880):104880. doi:10.1016/j.neuint.2020.104880
13. Chen X, Zhang T, Zhang Y (2020). Endoplasmic reticulum stress and autophagy in HIV-1-associated neurocognitive disorders. J Neurovirol, 26(6):824-833. doi:10.1007/s13365-020-00906-4
14. Bashir S, Banday M, Qadri O, et al (2021). The molecular mechanism and functional diversity of UPR signaling sensor IRE1. Life Sci, 265(118740):118740. doi:10.1016/j.lfs.2020.118740
15. Maurel M, Chevet E, Tavernier J, Gerlo S (2014). Getting RIDD of RNA: IRE1 in cell fate regulation. Trends Biochem Sci, 39(5):245-254. doi:10.1016/j.tibs.2014.02.008

16. Stewart C, Estrada A, Kim P, et al (2017). Regulation of IRE1α by the small molecule inhibitor 4μ8c in hepatoma cells. Endoplasmic Reticulum Stress Dis, 4(1):1-10. doi:10.1515/ersc-2017-0001
17. Cross BCS, Bond PJ, Sadowski PG, et al (2012). The molecular basis for selective inhibition of unconventional mRNA splicing by an IRE1-binding small molecule. Proc Natl Acad Sci U S A, 109(15):E869-78. doi:10.1073/pnas.1115623109
18. Sundermann EE, Bondi MW, Campbell LM, et al (2021). Distinguishing amnestic mild cognitive impairment from HIV-associated neurocognitive disorders. J Infect Dis, 224(3):435-442. doi:10.1093/infdis/jiaa760
19. Zhang K, Kaufman RJ (2008). From endoplasmic-reticulum stress to the inflammatory response. Nature, 454(7203):455-462. doi:10.1038/nature07203
20. Cirone M (2021). ER stress, UPR activation and the inflammatory response to viral infection. Viruses, 13(5). doi:10.3390/v13050798
21. Sims SG, Cisney RN, Lipscomb MM, Meares GP (2022). The role of endoplasmic reticulum stress in astrocytes. Glia, 70(1):5-19. doi:10.1002/glia.24082
22. Wheeler MA, Jaronen M, Covacu R, et al (2019). Environmental control of astrocyte pathogenic activities in CNS inflammation. Cell, 176(3):581-596.e18. doi:10.1016/j.cell.2018.12.012
23. Mo ZT, Liao YL, Zheng J, Li WN (2020). Icariin protects neurons from endoplasmic reticulum stress-induced apoptosis after OGD/R injury via suppressing IRE1α-XBP1 signaling pathway. Life Sci, 255(117847):117847. doi:10.1016/j.lfs.2020.117847
24. Chen D, Dixon BJ, Doycheva DM, et al (2018). IRE1α inhibition decreased TXNIP/NLRP3 inflammasome activation through miR-17-5p after neonatal hypoxic–ischemic brain injury in rats. J Neuroinflammation, 15(1). doi:10.1186/s12974-018-1077-9
25. Studencka-Turski M, Çetin G, Junker H, Ebstein F, Krüger E (2019). Molecular insight into the IRE1α-mediated type I interferon response induced by proteasome impairment in myeloid cells of the brain. Front Immunol, 10:2900. doi:10.3389/fimmu.2019.02900
26. Papandreou I, Denko NC, Olson M, et al (2011). Identification of an Ire1alpha endonuclease specific inhibitor with cytotoxic activity against human multiple myeloma. Blood, 117(4):1311-1314. doi:10.1182/blood-2010-08-303099
27. Bujisic B, Martinon F (2017). IRE1 gives weight to obesity-associated inflammation. Nat Immunol., 18(5):479-480. doi:10.1038/ni.3725
28. Zhao Y, Jiang Y, Chen L, et al (2020). Inhibition of the endoplasmic reticulum (ER) stress-associated IRE-1/XBP-1 pathway alleviates acute lung injury via modulation of macrophage activation. J Thorac Dis, 12(3):284-295. doi:10.21037/jtd.2020.01.45

Figures

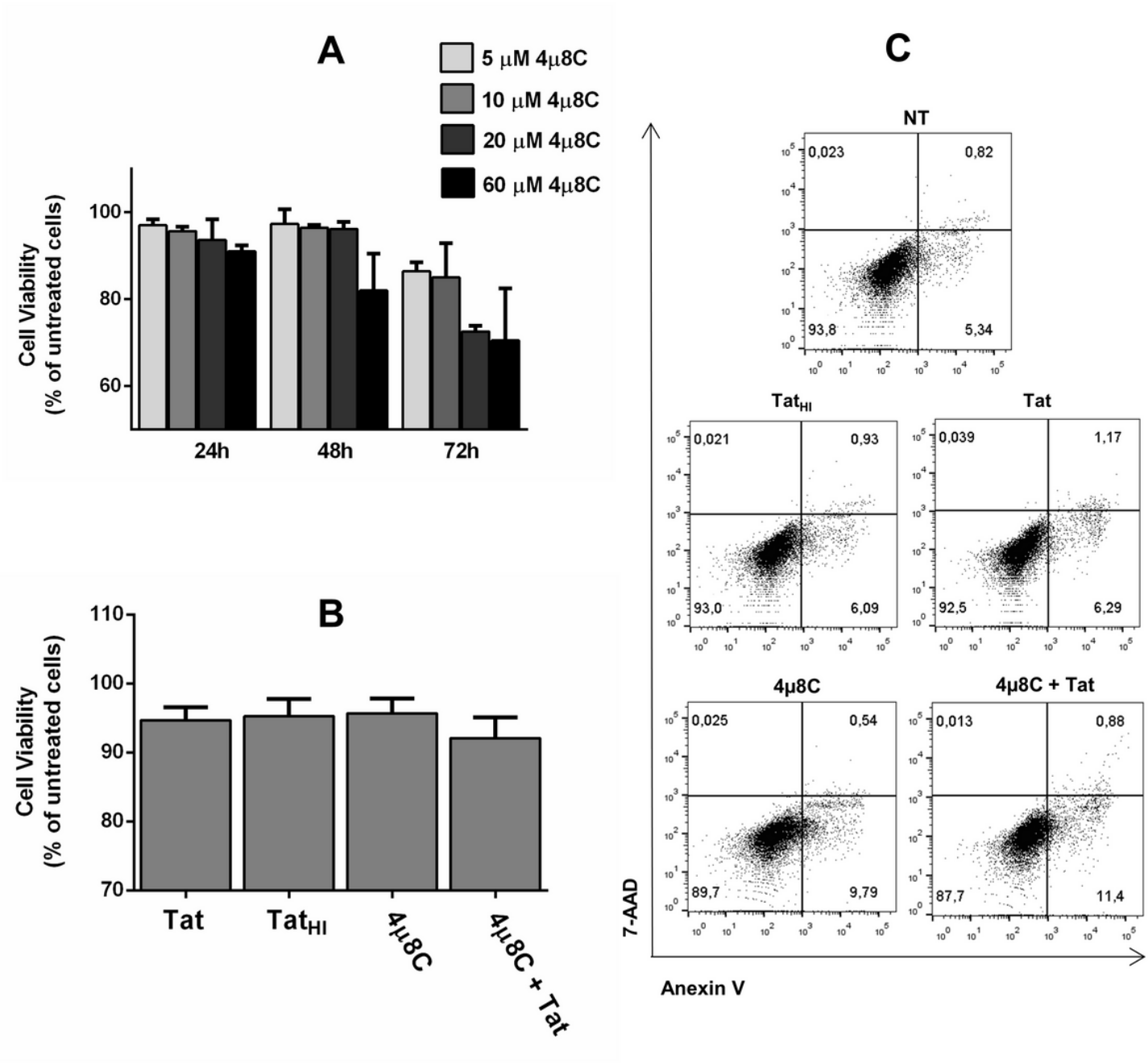

Figure 1

Effect of IRE1 inhibitor 4μ8C on cell viability and apoptotic fate of Tat-induced M1-like BV-2 cells. (A) BV-2 cells were incubated with increasing concentrations of IRE1 inhibitor 4μ8C at different time-points and cell viability was assessed by MTT assay. (B) BV-2 cells were cultured with 10 μM 4μ8C in presence or absence of 400 nM recombinant Tat for 48h and cell viability was estimated as described above. Data expressed as percentage of untreated cells ± SD. (C) Dot plot graphs showing apoptotic cell rates as percentage of BV-2 cells incubated with 10 μM 4μ8C in presence or absence of recombinant 400 nM Tat for 48h. Data acquired by flow cytometry after 7-AAD/Anexin V staining. Experimental controls were

performed with heat-inactivated Tat (Tat_{HI}, 400 nM) and untreated cells (NT). Data shown is representative of three independent experiments.

Figure 2

4μ8C downregulates HIV Tat-induced ER stress in BV-2 cells by interfering with the IRE1 pathway. (A) BV-2 cells were incubated for 48 h with 400 nM recombinant Tat with or without 10 μM 4μ8C, expression profile of IRE1 pathway-related genes was assessed by RT-qPCR and displayed as whisker-box plots of normalized expression ratio. (B) Expression of XBP-1u (unspliced form) and XBP-1s (spliced form) of Tat-treated BV-2 cells with or without 10 μM 4μ8C for 48 h evaluated by Western blotting. Bar graph shows the normalized band intensity values of Western blottings as mean ± SE. The figure was prepared from different fields of the same western blot images and this editing is indicated by the dotted line. Experimental controls were performed with heat-inactivated Tat (Tat_{HI}, 400 nM). Data are representative of two or three independent experiments. Statistical significance is indicated in relation to Tat-treated cells ($p < 0.05$*).

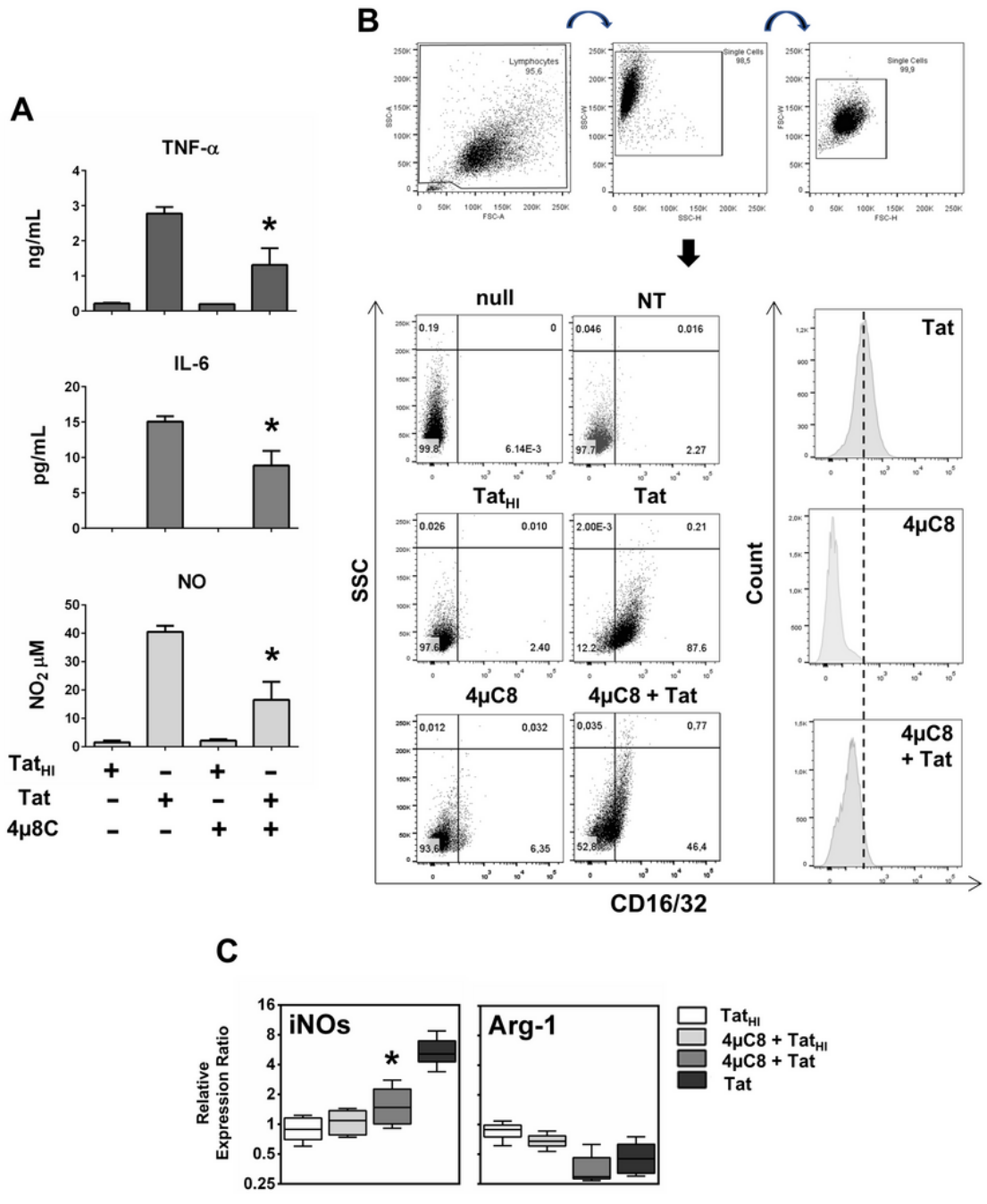

Figure 3

Inhibition of IRE1 RNase activity attenuates Tat-induced M1 phenotype in BV-2 cells. (A) Bar graphs show the levels of secreted TNF-α, IL-6 and NO of BV-2 cells incubated with 400 nM recombinant Tat with or without 10 µM 4µ8C for 48 h. Data acquired by CBA or Griess assay and expressed as mean ± SD. (B) Flow cytometry analysis of BV-2 cells incubated with 400 nM recombinant Tat with or without 10 µM 4µ8C for 48 h and labeled with CD16/32. Expression rates (dot plots) and fluorescence measurements

(histograms) are displayed. Null refers to unmarked cell control for flow cytometry assessments. Experimental controls were performed with heat-inactivated Tat (Tat_{HI}, 400 nM) and untreated cells (NT). (C) Tat-treated BV-2 cells (400 nM) were incubated with or without 10 μM 4μ8C for 48 h, iNOs and Arg-1 genes expression was assessed by RT-qPCR and displayed as normalized expression ratio. Experimental controls were performed with heat-inactivated Tat (Tat_{HI}, 400 nM). Data are representative of three independent experiments. Statistical significance is indicated in relation to heat-inactivated Tat-treated cells ($p < 0.05$*).